Modeling Fluid Flow Induced by *C. elegans* Swimming at Low Reynolds Number

Jonathan Gutierrez[1], Megan Sorenson[2], and Eva Strawbridge[3]

[1] St. Mary's University, San Antonio, TX 78228, USA
[2] Concordia University Irvine, Irvine, CA 92612, USA
[3] James Madison University, Harrisonburg, Virginia 22807, USA
strawbem@jmu.edu

Abstract. *C. elegans* have been extensively researched regarding locomotion. However, most mathematical studies have focused on body dynamics rather than the fluid. As the nematodes undulate in a sinusoidal fashion, they cause fluid movement that has been studied experimentally but not modeled computationally on this scale. Utilizing the Navier-Stokes equation, regularized stokeslets, and the method of images, we computed the dynamics of the surrounding fluid. Our results strikingly matched experimental outcomes in various ways, including the distance particles travelled in one period of undulation, as well as qualitatively and quantitatively matching velocity fields. We then implemented this method using video data of swimming *C. elegans* and successfully reproduced the fluid dynamics. This is a novel application of the method of regularized stokeslets that combines theory and experiment. We expect this approach to provide insight in generating hypotheses and informing experimental design.

Keywords: Applications of computing, computing with biology, *C. elegans*, low Reynolds number, regularized stokeslets, swimming.

1 Introduction

The past decade has evinced significant research into the locomotion of microorganisms, in particular that of the nematode *Caenorhabditis elegans* both theoretical and experimental [16,15,17,2,3,11,14]. However, while there have been a number of experimental investigations into the induced fluid movement of bacterial flagella or carpets [10,7], artificial helices [18], and nematodes [16], to the authors' knowledge, there has been little theoretical investigations into the induced fluid flows, particularly at the intermediate scale of *C. elegans*, a 1mm long, unsegmented round worm.

Fluid movement is potentially important for a number of reasons including mixing of either passive or active chemicals in the fluid [10,7,5], transport of nonzero volume particles [5], and swarm interactions of large numbers of organisms [9] all at low Reynolds number where viscosity, rather than inertia, dominates. In a viscosity dominated regime, where forcing is proportional to

A.-H. Dediu et al. (Eds.): TPNC 2014, LNCS 8890, pp. 71–82, 2014.

velocity rather than acceleration, mixing and flows are often counter intuitive due the reversibility. That is, any action which causes a flow in the fluid, if reversed *not necessarily at the same velocity* will effectively undo any flow, mixing, or propulsion. To overcome this reversibility and achieve forward locomotion, microorganisms utilize asymmetric motions such as corkscrewing of a helical flagella as with the bacteria *E. coli* or longitudinally asymmetric undulation as with *C. elegans*. In all of these cases, the organisms interact with the fluid which then interacts with either dissolved chemical species, suspended nonzero volume particles, or with other microorganisms to produce non-intuitive global behavior or results which are more than simply the sum of the individual motions of each swimmer separately.

Here we investigate these fluid motions first for an isolated swimmer in order to validate our computational model for the fluid and transport dynamics against experimental data in [16]. We use the method of regularized stokeslets in order to first model the induced fluid velocities of an artificial numerical swimmer and finally to extract fluid velocities from physical video data of a nematode swimming in a salt water solution. Even without fine tuning physical parameters, our model is able to reproduce experimental results including the appropriate decay of velocity magnitudes away from the forcing (i.e. organism) as well as qualitatively and quantitatively matching extremely well with PIV (particle image velocometry) measurements from [16] of the surrounding velocity fields.

By tracking particles or chemicals species in the fluid surrounding the multiple *C. elegans*, it may be possible to study mixing and chemical interactions theoretically. From this information, we hope to eventually inform experimental design and construct hypotheses which may be tested in the lab. The methods used here can also be adapted to computationally study the fluid flows induced by large numbers of swimming nematodes. Moreover, with some modifications to the computational swimmers it is also possible to further analyze organism-organism interactions in non-dilute populations in order to study the fluid dynamics contributions to swarm behavior.

2 Materials and Methods

The organism of study here is the nematode *C. elegans*, which are 1.06 ± 0.06 mm long and 80 μm in diameter [16]. Their wavelike movement has an average amplitude of 0.25 mm and a frequency of 2 Hz [16,2], meaning that a full beating cycle is completed in 0.5 seconds. The average forward swimming speed has been found to be 0.36 ± 0.06 mm/s by [16] and to be 0.12 mm/s at James Madison University's Wiggling Organism Research and Modeling (WORM) lab (the discrepancy here is likely due to the age, adult and L4 respectively, and size of the worms used in the respective experiments). The worms were analyzed swimming in M9, a salt water solution composed of $Na_2HPO_4 \cdot 7H_2O$, KH_2PO_4, NaCl, and NH_4Cl, between two slides separated by 0.15 mm coverslip spacers. The viscosity of M9 was measured in the WORM lab to be 1.596 cP at 20°C using a Brookfield DV-III LV Rheometer.

The induced fluid motion due to swimming *C. elegans* was studied using an in-house microscope designed based on the MRC Worm-Tracker microscope and implementing the Worm-Tracker software along with a strobing light source. Videos were taken at 10 and 15 frames per second of wild-type (N2) nematodes. The worms were maintained on agar plates using the standard OP50 *E. coli* strain at 20° C. These videos were processed and the centerlines extracted using Matlab©.

3 The Navier-Stokes Equation

The dynamics of incompressible Newtonian fluids are given by the Navier-Stokes equations,

$$-\nabla p + \mu \Delta \boldsymbol{u} = \rho \left(\frac{\partial \boldsymbol{u}}{\partial t} + \boldsymbol{u} \cdot \boldsymbol{\nabla} \boldsymbol{u} \right) - \boldsymbol{f} \ , \tag{1}$$

$$\boldsymbol{\nabla} \cdot \boldsymbol{u} = \boldsymbol{0} \ , \tag{2}$$

where $-\nabla p$ is the pressure gradient, μ the dynamic viscosity, $\nabla = \left(\frac{\partial}{\partial x}, \frac{\partial}{\partial y}, \frac{\partial}{\partial z} \right)$ is the gradient operator, $\Delta = \frac{\partial^2}{\partial x^2} + \frac{\partial^2}{\partial y^2} + \frac{\partial^2}{\partial z^2}$ is the three dimensional Laplacian operator, $\boldsymbol{u}$ the flow velocity, ρ the fluid density. Finally, $-\boldsymbol{f}$ represents external forces due to, for example, a body moving in the fluid. We will use the method of regularized stokeslets (described later in the text) to determine an appropriate representation for $\boldsymbol{f}$. Equation (2) represents the incompressibility condition. Because all solutions of interest here are aqueous and water is incompressible this condition plus and appropriate representation of $\boldsymbol{f}$, closes the system of equations above.

It is worth noting that the terms of the Navier-Stokes equation yield the individual forces in the system where $\mu \Delta \boldsymbol{u}$ is the viscous force and $\rho \left(\frac{\partial \boldsymbol{u}}{\partial t} + \boldsymbol{u} \cdot \boldsymbol{\nabla} \boldsymbol{u} \right)$, the only component which is nonlinear in velocity, corresponds to the inertial forces. In the next section we will argue that for the regime of interest, the nonlinear inertial terms may be neglected, reducing the system to a linear one and enabling the use of regularized stokes ets and the method of images.

3.1 Nondimensionalization

We have previously referred to *C. elegans* as a low Reynolds number swimmer, meaning that we expect this to be a viscosity dominated regime. The Reynolds number is effectively the ratio of the size of inertial to viscous forces. If this ratio is small, viscosity dominates; if it is large, inertia dominates; and if it is approximately 1, then both should remain important. Inertia works to keep an object going at a constant velocity while viscosity is the resistance of the fluid to flow [13]. At this point it is salient to note that 1mm, while small, is not microscopic and can be seen with the naked eye. Additionally, the viscosity of M9 is only about 1.5 times that of water, which is most certainly not a viscous

fluid. Therefore it is imperative to determine the Reynolds number for these experiments.

For the nondimensionalization of the Navier-Stokes equation, the unknowns are separated into two components, units and scalars, allowing units to be removed in order to compare the relative importance of inertial and viscous forces. We use p = $P_0\hat{p}$, x = L$\hat{x}$, y = L$\hat{y}$, z = L$\hat{z}$, t = T$\hat{t}$, and $\boldsymbol{u} = \frac{L}{T}\hat{u}$, where the hats indicate the nondimensional variables. Here $\frac{L}{T}\hat{u}$ is the natural component for velocity. Additionally, we chose the units of pressure to be $\frac{\mu}{T}$. Utilizing these substitutions and with some simplification (1) becomes

$$-\hat{\nabla}\hat{p} + \hat{\Delta}\hat{u} = \frac{\rho L^2}{T\mu}\left(\frac{\partial \hat{u}}{\partial \hat{t}} + (\hat{u}\cdot\hat{\nabla}\hat{u})\right) \quad , \tag{3}$$

where the highlighted term is the Reynolds number.

By rewriting $V = \frac{L}{T}$ and $\eta = \frac{\mu}{\rho}$, the Reynolds number becomes $\frac{LV}{\eta}$, where L and V represent a characteristic length and velocity of the system respectively and η represents dynamic viscosity. Using the appropriate parameters for *C. elegans* we find $\frac{LV}{\eta} = \frac{(1\text{mm})(0.12\frac{\text{mm}}{\text{s}})}{1.596\text{cP}} = 0.075$, which is much less than one. The inertial terms can be dropped, simplifying (1) to a linear system which is called the Stokes equation. The Stokes equation always possesses a unique solution and moreover, linearity allows the calculation of the velocity due to different forces to be summed separately rather than solved simultaneously.

3.2 Regularized Stokeslets

As previously indicated, modeling the fluid flow induced by the locomotion of swimming nematodes is appropriate using the forced Stokes equation which is given by

$$-\nabla p + \mu\Delta\boldsymbol{u} = -\boldsymbol{f}, \tag{4}$$

where p and $\boldsymbol{u}$ are the nondimensionalized pressure and velocity respectively after dropping the hat notation, and $\boldsymbol{f}$ is the nondimensional external forcing acting on the fluid. When $\boldsymbol{f}$ represents a point force we have $\boldsymbol{f} = \boldsymbol{g}\delta(\boldsymbol{X})$ where δ is the Dirac delta function and $\boldsymbol{X} = \boldsymbol{x} - \boldsymbol{x}_0$ is the vector difference between a position $\boldsymbol{x}$ and the location of the point force at $\boldsymbol{x}_0$. Here the position of the point forces lie along the body of the swimmer. For the delta function point force (4) has an exact solution which is given by the stokeslet. While this solution is exact at all locations away from the object, it is singular at the location $\boldsymbol{x}_0$. Numerically this presents a problem when the point forces are distributed along a curve in three-dimensions as is desired in this case when modeling a slender body because the velocity field becomes infinite on the filament itself [4,6].

To resolve the numerical issues due to this singularity, rather than using delta functions the forcing is chosen to be represented by smooth but localized force which is defined everywhere, $\boldsymbol{f} = \boldsymbol{g}\phi_\epsilon(\boldsymbol{X})$. Generally this smooth, radially symmetric function, ϕ_ϵ, is referred to as a "blob" function and is required to decay sufficiently fast. That is, we shall require $\int_0^\infty r^2\phi_\epsilon(r)dr = \frac{1}{4\pi}$. The parameter ϵ

controls where the majority of the force is concentrated and is generally chosen to represent a physical quantity such as the radius of the filamentary object, here the radius of the worm, 40μm. With the forcing given by this smooth function, (4) has an exact solution given by the regularized stokeslet [5]. A typical blob function is of the form $\phi_\epsilon(r) = \frac{15\epsilon^4}{8\pi(r^2+\epsilon^2)^{7/2}}$. Then the corresponding biharmonic function to this regularized stokeslet is given by$\Delta^2 B_\epsilon(r) = \phi_\epsilon(r)$ so the regularized stokeslet is then

$$\frac{1}{8\pi} S_\epsilon(\boldsymbol{X}) = \left(-\frac{B_\epsilon''(r)}{r} - B_\epsilon''(r)\right)\boldsymbol{I} + \left(\frac{rB''(r) - B_\epsilon'(r)}{r^3}\right)\boldsymbol{X}\boldsymbol{X}. \tag{5}$$

3.3 Method of Images

Because all experimental data to which these computations will be compared have walls, we implemented a version of the regularized stokeslet which also contains solutions using the method of images. The method of images is a common mathematical approach to enforce wall boundary conditions in one direction for linear partial differential equations, as in this case with a floor. In essence, to ensure zero flow through the wall due to a force in the fluid, an imaginary force is added which mirrors the real force on the other side of the wall. These two forces then effectively "cancel" each other out. This procedure is technically more complicated for the regularized stokeslet and requires the additional use of a doublet and potential dipole at the mirror image point as well but has been previously obtained by [1] and is implemented here. A complete treatment of the method of images for regularized stokeslets is beyond the scope of this paper but can be found in compete detail in [1].

4 The Model Nematode

Our initial investigations implemented a computationally artificial model of *C. elegans* given by

$$x = \left[2\pi ks + \iota\omega t\right]/L_{arc}\ , \tag{6}$$

$$y = \left[A\sin\left(\frac{2\pi s}{\lambda} + \omega t\right)e^{\alpha s}\right]/L_{arc}\ . \tag{7}$$

The parameters $Ae^{\alpha s}$ control the maximum amplitude. The value of A is chosen based on α, which controls the decay of amplitude through the worm from head to tail. However, it should be noted that A is not a direct reflection of the maximum amplitude. The parameter λ is the wave length, s is the parameterization variable, and ω is the oscillation frequency. *C. elegans*' forward displacement is not equal to ω, so a slip parameter ι was introduced. To account for the length, 1 mm, of the worm, we normalize by the arc length L_{arc} of the function at each time.

To use the method of regularized stokeslets, we implemented a blob parameter of $d = 40$ μm equally spaced along the nematode so that there were $\lfloor 1/2d \rfloor$

(13 in this case) blobs. Adjacent forces positioned too far apart would result in our worm having holes, allowing fluid flow through the centerline. Conversely, the blobs cannot be too close together because overlapping blobs would create a total force much greater than the actual force induced by the worm [5].

5 Results

5.1 Velocity Field

Using regularized stokeslets, the method of images, and knowing the position and velocity of the blob forces, the forcing on, and therefore velocity of the fluid can be computed exactly at any point in time and space. *That is, this is a grid free method.* This allows us to compute the velocity vector field around the worm as is shown in Fig. 1a. Here we can see that the velocity vectors (which are denoted as lines with circles at the heads) are largest near the body as predicted, particularly around areas of greater body displacement as was observed in the experiments of [16,8]. Additionally, circular trajectories rotating in alternating directions are observed. These circular regions remain near the body, opposed to traveling out into the fluid, a characteristic of low Reynolds number swimmers' fluid dynamics [16].

Figure 1b shows a color map of the velocity magnitude in a grid surrounding the nematode as was produced from the experimental data of [16]. Larger velocities are seen near the areas of greater body displacement and circular flow regions remain present. Once again, the theoretical nematode is consistent with the experimental results. When similar parameters as those shown in the figures of [16] were implemented, the maximum magnitudes were within approximately 10 μ m/s. Additionally, we found that the magnitudes of the velocities vary significantly with fluctuation in the nematode length, frequency, and wavelength.

5.2 Velocity Magnitude and Distance from the Wall

We computed the normalized average velocity magnitude as a function of the the normalized distance r/L from the worm (here L = 1mm) averaged over the length of the worm and one full beat period. Because the bulk fluid flow is zero, we expect the velocity to decay to zero as our observations move away from the worm. Figure 2a depicts the calculation scheme and Fig. 2b indicates the theoretically predicted exponential decay rate, $e^{-2\pi r/\lambda}$, as the solid blue line [12]. This method is consistent with the computations of [5] and the experimental observations of [18] with rotating metal helices.

The experimental techniques of [16] specifically measured the velocity magnitudes of the nematodes at 300 μm (roughly $7d$, where d is the nematode radius) from the bottom wall of the fluid containing cell. Our numerical method enables us to examine the effect of distance from the wall and its impact on the fluid behavior. We computed the velocity magnitudes as a function of distance from the nematode's maximum amplitude (as shown in Fig. 2a) for heights ranging

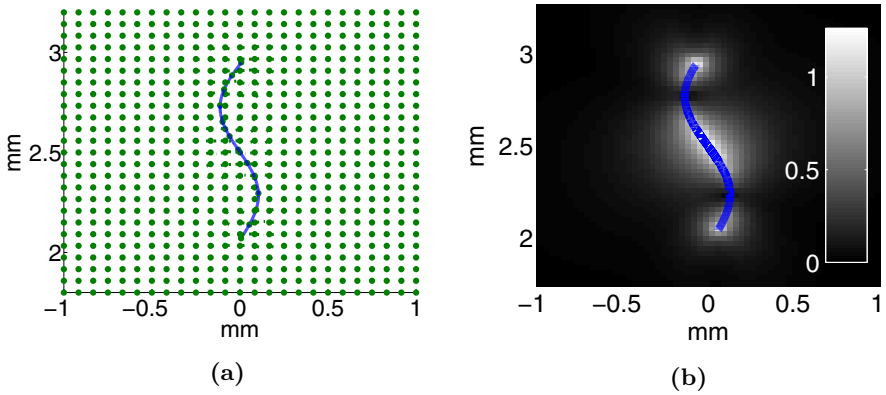

Fig. 1. (a) The velocity vector field shows the direction of fluid surrounding the worm and a rough magnitude of each vector. The circles indicate position at which the velocity vectors were calculated. (b) The grayscale bar indicates the magnitude of the velocity vector.

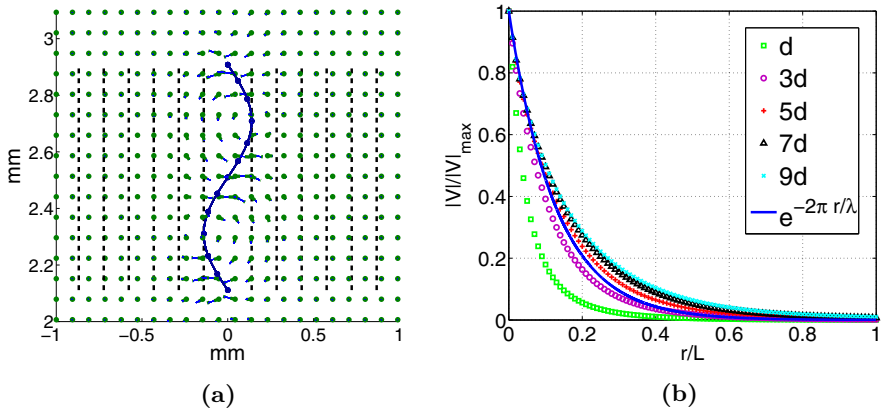

Fig. 2. (a) Along each of the dashed vertical lines we computed the normalized flow velocity magnitudes at a distance, r, away from our model worm ($L = 1$ mm). The circles indicate position at which the velocity vectors were calculated. (b) Velocity magnitudes are observed as the distance from the nematode increases. The decaying velocities at different heights away from the wall are then plotted. The solid line shows the predicted outcome from [12]

from d to $10d$ above the bottom wall. When the distance is roughly 300 μm, the numerical results (Fig. 2b labeled in black) lie just above the the predicted decay, $e^{-2\pi r/\lambda}$, of [12], and are nearly identical to the experimental results of [16].

Additionally, we were able to calculate X_{thres}, the normalized distance from the artificial worm where velocity magnitudes fall below ten percent of their respective maximums. As the distance from the wall increases, these values appear to converge to 0.5039. When the maximum velocities $\mid V \mid_{max}$ for each of these heights were calculated, we found that as the distance from the wall increases, $\mid V \mid_{max}$ increases as well and also appears to converge to 0.7853 mm/sec.

To the authors' knowledge, the relationship between velocity decay or maximum velocity produced as a function of distance from a wall has not previously been examined and our experiments predict that expected decay rate of [12] does not accurately describe normalized fluid velocity magnitudes generated when a wall is present but at a substantial distance from the swimming organism. This represents a very testable hypothesis that we hope to investigate further both numerically and experimentally.

5.3 Particle Tracking

Fluid particles located in the plane of the worm's motion were tracked and these particle paths are shown in Fig. 3. The circular flow patterns are again evident and the particles are seen to have moved the greatest distance near the regions of greatest body displacement, indicating that these circular regions are characteristic of streamlines, not simple vector fields at a snapshot in time. We wanted to ensure that our particle movement was an accurate representation of the actual change in position. To test this, we tracked particles directly on the worm. If computed exactly, particle on the body will remain on the nematode for all time. However, we expect to observe first order error in the time evolution of particle location.

Because the integration scheme used is first order in time, as the time step dt is decreased, the error should decrease proportionally. To check our numerical method we computed the euclidian distance between the actual location of fluid particles initialized on the worm itself, and the point where it should have been positioned on the worm. This distance is recorded in Table 1. At T = 0.1 (roughly the end time used for the particle tracking in Fig. 3) and 0.5 seconds (a full beat cycle), we see from this table that we do in fact have first order convergence. However, as the end time is increased, the method for tracking particles does not continue to show the appropriate relationship. The increased error is likely caused by the method of evenly distributing the blob forces on the sinusoidal curve as a function of time. However, our model works well for all periods of time for which experimental data exists with which to compare.

Particles paths were also plotted where color corresponds to a total distance traveled (Fig. 4). From this figure we see that the maximum distance a fluid particle traveled is approximately 50 μm. This is strikingly consistent with the experimental data from [16] which was produced using PIV and suspended

florescent particles. We found that the distance each particle traveled was effected greatly by the physical parameters such as the length of the nematode, beat frequency, and wave length, indicating that further investigation into this is needed in order to determine upper bounds for mixing, and compare with real experimental situations.

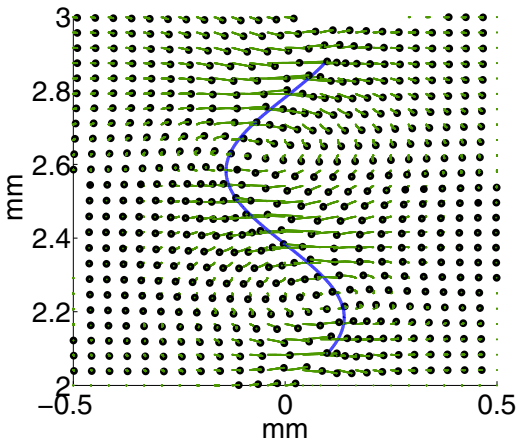

Fig. 3. Particles are tracked for 0.125 seconds with a dt of 0.001 as the worm swims through the fluid where the particles themselves are plotted as dots at the ending time

Table 1. The relationship between time step size and error decrease is the correct proportion for T = 0.1 and T = 0.5 seconds

(a) Total Time = 0.1

dt	distance	$\frac{dd_{n+1}}{dd_n}$
0.1	0.0071	-
0.05	0.0035	2.0014
0.025	0.0018	2.0018
0.0125	0.0009	2.0030
0.00625	0.0004	2.0057

(b) Total Time = 0.5

dt	distance	$\frac{dd_{n+1}}{dd_n}$
0.1	0.0070	-
0.05	0.0035	2.0193
0.025	0.0017	2.0371
0.0125	0.0008	2.0757
0.00625	0.0004	2.1631

6 From Theory to Experiment

After validating our computational model with the numerical artificial swimmer, we extended this work to experimental data obtained in our own lab. Videos were

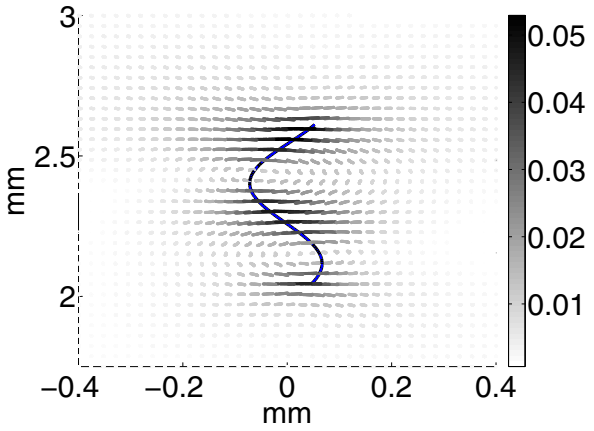

Fig. 4

Fig. 5. Particles are traced for 0.06 seconds with a time step of 0.002. The color bar indicates the magnitude of displacement in mm.

taken of L4 *C. elegans* for four seconds at ten frames per second. The centerline of these worms was extracted and normalized into mm, as seen in Fig. 6a. The worm centerlines were then divided up into the 13 blob forces used to create the velocity field around the nematode. Two consecutive frames were plotted, and the velocities were calculated by tracking the distance each blob traveled and dividing this the change in time between frames. Figure 6b depicts the worm's initial position plotted with a dashed line and the final position plotted as a solid line. Three regions of higher velocity magnitude are present, along with the circular motion of the velocity vectors, once again consistent with the results found by [16]. While the velocity magnitudes obtained here are slightly larger than those found by [16], we believe this is due the significant variation of movements between worms as well as over time. This parameter dependence is a subject of future study.

7 Conclusion

We implemented an algorithm that utilizes regularized stokeslets and the method of images to track the fluid dynamics around a swimming *C. elegans* at low Reynolds number. Results were obtained using both a computationally artificial worm and experimentally obtained video data to study the fluid dynamics associated with nematode locomotion. Particles carried by the fluid were tracked numerically, reproducing experimental outcomes with respect to particle displacement. The velocity fields as well as the velocity magnitudes as a function of lateral distance from the worm also match both qualitatively and quantitatively with the experiments of [16] and the theoretical predictions of [12]. Moreover, by

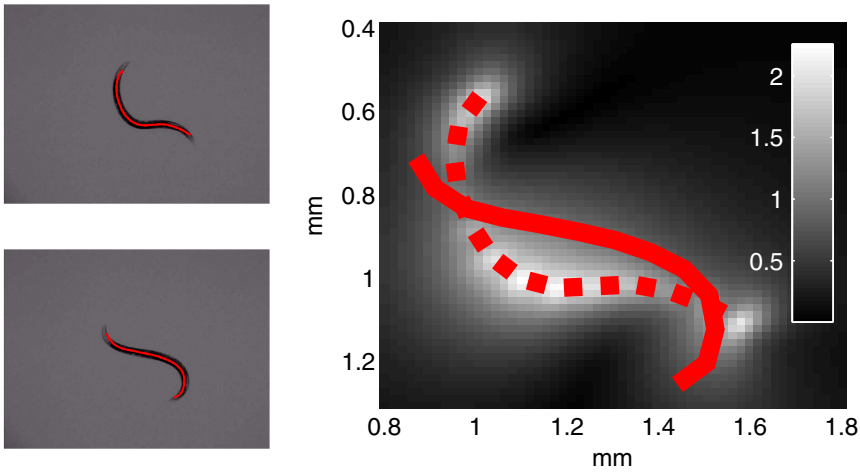

Fig. 6. (a) *C. elegans* photographs with extracted centerline gathered in our lab. (b) The color velocity field based on *C. elegans* movement as the worm moves from the dashed line to the solid line over 0.1 seconds. The grayscale color bar indicates magnitude of the velocity vectors in mm/s.

computationally studying the impact of experimentally relevant boundaries (i.e. the bottom of the fluid chamber), we can predict this decay rate as a function of distance from this wall.

In future work we hope to extend this research to study the precise relationship between flow features and the physical and locomotive parameters of real nematodes (e.g. body length, wave length, longitudinal asymmetry, wave speed, etc.) as well as to include multiple swimmers in order to analyze fluid dynamics contributions of swarm behavior through organism-organism interaction in non-dilute environments. In order to study complex patterns and behaviors associated with dense or non dilute populations of swimmers (i.e. potential swarms) in fluids, a clear understanding of the dynamic role of the *fluid* in this behavior and communication between organisms is needed. Additionally, this method can be used to track particles or chemical species in fluids to further investigate microscopic mixing as well as the chemical processes aided by active flow. This is particularly applicable to the construction of microfluidic devices and mixing using bacterial carpets [10].

Acknowledgements. This research was partially funded by NSF grant number 1004516, and James Madison University Mathematics and Statistic Department provided funding for the WORM lab. Charles Wolgemuth and Karin Leiderman contributed the original centerline and regularized stokeslets programs respectively.

References

1. Ainley, J.S., Durkin, S., Embid, R., Boindala, P., Cortez, R.: The method of images for regularized stokeslets. Journal of Computational Physics 227, 4600–4616 (2008)
2. Berman, R.S., Kenneth, O., Sznitman, J., Leshansky, A.M.: Undulatory locomotion of finite filaments: lessons from *Caenorhabditis elegans*. New Journal of Physics 15, 075022 (2013)
3. Berri, S., Boyle, J.H., Tassieri, M., Hope, I.A., Cohen, N.: Forward locomotion of the nematode *C. elegans* is achieved through modulation of a single gait. HFSP Journal 3, 186–193 (2009)
4. Bouzarth, E., Minion, M.: Modeling slender bodies with the method of regularized stokeslets. Journal of Computational Physics 230, 3929–3947 (2011)
5. Buchman, A.L., Fauci, L.J., Strawbridge, E.M., Zhao, L.: Flow included by bacterial carpets and transport of microscale loads. IMA Volume: Applications of Dynamical Systems in Biology and Medicine (to appear, 2014)
6. Cortez, R.: The method of regularized stokeslets. SIAM Journal on Scientific Computing 23, 1204–1225 (2001)
7. Darnton, N., Turner, L., Breuer, K., Berg, H.: Moving fluid with bacterial carpets. Biophysical Journal 86, 1863–1870 (2004)
8. Gray, J., Lissmann, H.W.: The locomotion of nematodes. Journal of Experimental Biology 41, 135 (1964)
9. Ishikawa, T., Pedley, T.J.: Coherent structures in mololayers of swimming particles. Physical Review Letters 100, 088103 (2008)
10. Kim, M., Breuer, K.: Use of bacterial carpets to enhance mixing in microfluidic systems. Journal of Fluids Engineering 46, 139 (2007)
11. Korta, J., Clark, D.A., Gabel, C.V., Mahadevan, L., Samuel, A.D.T.: Mechanosensation and mechanical load modulate the locomotory gait of swimming *C. elegans*. The Journal of Experimental Biology 210, 2382–2389 (2007)
12. Lighthill, J.: Flagellar hydrodynamics. SIAM Reviews 18, 161 (1976)
13. Purcell, E.M.: Life at low reynolds number. American Journal of Physics 45, 3 (1977)
14. Shen, X.N., Arratia, P.E.: Undulatory swimming in viscoelastic fluids. Physical Review Letters 106, 208101 (2011)
15. Sznitman, J., Prashant, K., Purohit, P., Lamitina, T., Arratia, P.E.: Material properties of *Caenorhabditis elegans* swimming at low reynolds number. Biophysical Journal 98, 617–626 (2010)
16. Sznitman, J., Shen, X., Sznitman, R., Arratia, P.E.: Propulsive force measurements and flow behavior of undulatory swimmers at low reynolds number. Physics of Fluids 22, 121901 (2010)
17. Sznitman, R., Gupta, M., Hager, G.D., Arratia, P.E., Sznitman, J.: Multi-environment model estimation for motility analysis of Caenorhabditis elegans. PLoS One 5, e11631 (2010)
18. Zhong, S., Moored, K.W., Pinedo, V., Garcia-Gonzalez, J., Smits, A.J.: The flow field and axial thrust generated by a rotating rigid helix at low reynolds number. Experimental Thermal and Fluid Science 46, 1–7 (2013)